The field-free Josephson diode in a van der Waals heterostructure

Wu, Heng; Wang, Yaojia; Xu, Yuanfeng; Sivakumar, Pranava K.; Pasco, Chris; Filippozzi, Ulderico; Parkin, Stuart S.P.; Zeng, Yu Jia; McQueen, Tyrel; Ali, Mazhar N.

DOI
10.1038/s41586-022-04504-8

Publication date
2022

Document Version
Final published version

Published in
Nature

Citation (APA)
Wu, H., Wang, Y., Xu, Y., Sivakumar, P. K., Pasco, C., Filippozzi, U., Parkin, S. S. P., Zeng, Y. J., McQueen, T., & Ali, M. N. (2022). The field-free Josephson diode in a van der Waals heterostructure. *Nature*, *604*(7907), 653-656. https://doi.org/10.1038/s41586-022-04504-8

Article

The field-free Josephson diode in a van der Waals heterostructure

https://doi.org/10.1038/s41586-022-04504-8

Received: 29 March 2021

Accepted: 2 February 2022

Published online: 27 April 2022

Check for updates

Heng Wu[1,2,3,6]✉, Yaojia Wang[1,3,6], Yuanfeng Xu[1,4], Pranava K. Sivakumar[1], Chris Pasco[5], Ulderico Filippozzi[3], Stuart S. P. Parkin[1], Yu-Jia Zeng[2], Tyrel McQueen[5] & Mazhar N. Ali[1,3]✉

The superconducting analogue to the semiconducting diode, the Josephson diode, has long been sought with multiple avenues to realization being proposed by theorists[1–3]. Showing magnetic-field-free, single-directional superconductivity with Josephson coupling, it would serve as the building block for next-generation superconducting circuit technology. Here we realized the Josephson diode by fabricating an inversion symmetry breaking van der Waals heterostructure of $NbSe_2$/Nb_3Br_8/$NbSe_2$. We demonstrate that even without a magnetic field, the junction can be superconducting with a positive current while being resistive with a negative current. The ΔI_c behaviour (the difference between positive and negative critical currents) with magnetic field is symmetric and Josephson coupling is proved through the Fraunhofer pattern. Also, stable half-wave rectification of a square-wave excitation was achieved with a very low switching current density, high rectification ratio and high robustness. This non-reciprocal behaviour strongly violates the known Josephson relations and opens the door to discover new mechanisms and physical phenomena through integration of quantum materials with Josephson junctions, and provides new avenues for superconducting quantum devices.

Reciprocity in charge transport describes the symmetric behaviour of current with voltage; the magnitude of the current generated by a positive voltage is the same as that generated by a negative voltage[4]. Violating reciprocity, that is, non-reciprocal behaviour, forms the basis for numerous important electronic devices such as diodes, a.c./d.c. converters, photodetectors, transistors and so on[5,6]. A well-known example of a non-reciprocal device is the p–n junction, formed by the interface of a p- and n-doped semiconductor, which shows an asymmetric current-voltage characteristic (IVC) without applied magnetic field (B) and is widely used in various semiconducting technologies including logic and computation[7].

So far, in the superconducting regime, field-induced non-reciprocal behaviour has been seen in non-centrosymmetric superconductors[8–10] and two-dimensional electron gases[11], and multiple mechanisms for this phenomenon have been proposed[9,12,13]. All require an applied magnetic field to achieve simultaneous breaking of inversion symmetry and time reversal symmetry[14–16] so that with sufficient magnetic field strength, the critical current required to destroy the superconducting state in one direction can be different from that in the other direction[8]. Non-reciprocal superconductivity without an applied magnetic field as not yet been observed either in a bulk superconductor or a superconducting junction, such as a Josephson junction (JJ).

In particular, the JJ is also known to show reciprocal behaviour, as can be seen by the Josephson relations[17,18]. JJs are typically formed by two superconducting electrodes bridged by a non-superconducting barrier composed of classical materials (AlO_x, Cu and so on)[19,20]. However, integrating new quantum materials as the barriers in JJs may lead to anomalous behaviour violating the Josephson relations (such as non-reciprocal behaviour) and is of fundamental and technological interest. Creating a superconducting analogue to the semiconducting diode, a field-free 'Josephson diode' (JD), allowing supercurrent in one direction but normal current in the other direction in the absence of an applied magnetic field, is an open challenge.

One approach is to look for non-reciprocal IVCs in superconducting systems that only break inversion but not time reversal symmetry. Recently, JJs with only inversion symmetry breaking were predicted to show non-reciprocal IVCs owing to the formation of a Mott-insulating depletion region at the interface of p-doped and n-doped superconductors[2]. As JJs form the basis of a variety of important technologies[21,22] including superconducting quantum interference devices, superconducting quantum computing bit (qubits) and rapid single flux quantum devices[23–25], the realization of the JD will have a substantial impact on superconducting electronics.

Here we report the realization of the field-free JD in an inversion symmetry breaking the van der Waals heterostructure of $NbSe_2$/Nb_3Br_8/$NbSe_2$. An asymmetric IVC, with sharp superconducting transitions, is seen at a zero magnetic field indicating its field-free JD behaviour. A superconducting half-wave rectification of a square-wave excitation is demonstrated with a large rectification ratio, ultralow switching current density and highly stable performance. Moreover, the ΔI_c versus B, presents a symmetric behaviour, unlike the antisymmetric response seen in previous systems[8], further proving its

[1]Max Planck Institute of Microstructure Physics, Halle, Germany. [2]College of Physics and Optoelectronic Engineering, Shenzhen University, Shenzhen, China. [3]Kavli Institute of Nanoscience, Delft University of Technology, Delft, The Netherlands. [4]Department of Physics, Princeton University, Princeton, NJ, USA. [5]Johns Hopkins University, Baltimore, MD, USA. [6]These authors contributed equally: Heng Wu, Yaojia Wang. ✉e-mail: wuhenggcc@gmail.com; m.n.ali@tudelft.nl

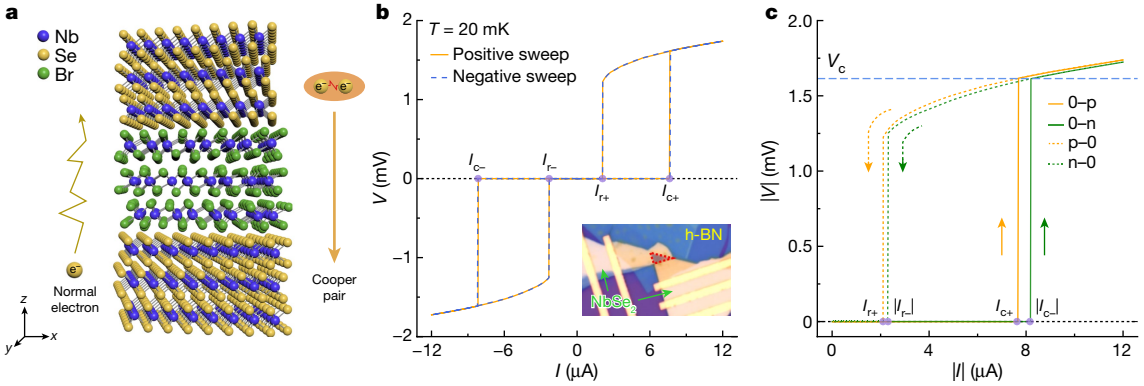

Fig. 1 | Schematic and superconductivity of the JD at zero field. a, Schematic of a JD in a vertical JJ architecture, consisting of an $NbSe_2/Nb_3Br_8/NbSe_2$ sandwich. The junction lacks inversion symmetry along the *z* direction, and can show normal conduction in one direction but superconductivity in the other (Cooper pair conduction). **b**, *V*–*I* curves measured by sweeping positive (orange solid line) and sweeping negative (blue dashed line), as defined in the main text. Inset, a typical device architecture; the red triangle outlines the JJ geometry created by the overlapping flakes. **c**, *V*–*I* curves with positive sweep; the orange solid and dashed lines correspond with the 0–p and p–0 branches, respectively, and the green solid and dashed lines correspond with the 0–n and n–0 branches, respectively. The purple dots mark the position of I_{c+}, $|I_{c-}|$, I_{r+} and $|I_{r-}|$ and the blue dashed line shows the critical voltage V_c.

field-free nature. The field-free JD effect may lie in the asymmetric tunnelling of supercurrent across the tunnel barrier, and the inversion symmetry breaking of the junction is confirmed by antisymmetric second-harmonic peaks. The effect shown here may be extended to a variety of material systems and architectures, particularly using van der Waals materials, for the advancement of future superconducting electronics and quantum devices. Also, this study shows how the interplay between symmetry breaking, new tunnel barrier materials and superconducting electrodes can lead to new or anomalous Josephson phenomena in JJs, opening the door to a variety of fundamental and applied research directions.

Experimental data

We fabricated vertical JJs by sandwiching an Nb_3Br_8 thin flake with thin flakes of $NbSe_2$ as shown in Fig. 1a. Nb_3Br_8 is a van der Waals quantum material that crystallizes in the $R\bar{3}m$ space group at low temperature and its unit cell is composed of six layers of Nb-Br edge-sharing octahedra[26,27] with inversion centres lying between adjacent layers (Extended Data Fig. 1a). The inversion symmetry is preserved in even-layered Nb_3Br_8 but broken in odd-layered Nb_3Br_8. Additionally, Nb_3Br_8 was shown to have a singlet magnetic ground state[27] and moderate band gap like its sister material, Nb_3Cl_8[27–30] (see Methods and Extended Data Fig. 5 for magnetoresistance characterization of the Nb_3Br_8 thin flakes). The $NbSe_2/Nb_3Br_8/NbSe_2$ heterostructures were fabricated by the dry transfer method[31] (Methods) and capped by a top hexagonal boron nitride (h-BN) to avoid degradation, as a typical device in the inset of Fig. 1b shows. Here $NbSe_2$ flakes with thickness about 28–37 nm are used as superconducting electrodes, rotated by arbitrary angles with respect to each other, breaking inversion symmetry of the JJ, and a thin flake of Nb_3Br_8 with thickness of 2.3 nm (three layers) is used as the tunnel barrier.

When cooling the junction to 20 mK in zero field, a sudden drop to zero resistance at $T_c = 6.6$ K is observed, as shown in Extended Data Fig. 1b. Figure 1b investigates the voltage versus current (*V*–*I*) behaviour, measured by sweeping the d.c. current at 20 mK (see *V*–*I* curves at different temperatures in Extended Data Fig. 1c). We emphasize that the measurement of the *V*–*I* curves contains four branches; sweeping the current from zero to positive (0–p), from positive back to zero (p–0), from zero to negative (0–n) and from negative back to zero (n–0). These four branches can be measured in the above order (defined as the positive sweep), or in reverse order, 0–n, n–0, 0–p and p–0 (defined as the negative sweep). Figure 1b shows *V*–*I* curves of the positive sweep and the negative sweep; both of them show hysteresis, as expected, arising from the capacitance induced different critical currents when breaking (I_c) compared with returning (I_r) to the superconducting state[1]. Note that the properties measured here all come from the JJ itself as the maximum current applied here is much smaller than the critical current of thick $NbSe_2$ (a few milliamps)[32]. The two curves lie precisely on top of each other meaning that the positive versus negative sweep order does not affect the *V*–*I* response. However, the I_c and I_r in the positive current regime (labelled I_{c+} and I_{r+}) can be compared with those in the negative current regime (labelled I_{c-} and I_{r-}). For reciprocal transport, as is expected for a conventional JJ without magnetic field, there should be no difference between I_{c+} versus $|I_{c-}|$ or I_{r+} versus $|I_{r-}|$.

Figure 1c shows the absolute values of I_{c+} and I_{r+} as well as I_{c-} and I_{r-} of the positive sweep. Immediately evident is that I_{c+} and I_{r+} are not equal to their negative current counterparts, with a ΔI_c ($\Delta I_c = |I_{c-}| - I_{c+}$) roughly 0.5 μA and a smaller ΔI_r roughly 0.1 μA, indicating the non-reciprocal *V*–*I* response in our JJ. It is important to note that these differences are intrinsic properties of the JJ rather than an extrinsic Joule heating effect (see discussion in the Methods). The different absolute values of I_{c+} and I_{c-} combined with the sharp superconducting transition indicate that when the applied current is in between I_{c+} and $|I_{c-}|$, the junction would show superconducting behaviour with a negative current but normal conducting behaviour with a positive current.

On the basis of this idea, we demonstrated half-wave rectification at zero field, as shown in Fig 2a. Because the I_{c+} and $|I_{c-}|$ being 7.61 and 8.14 μA, respectively, we applied a square-wave excitation (Fig 2a, top panel) with an amplitude of 7.9 μA at a frequency of 0.1 Hz. As shown in the bottom panel of Fig 2a, the junction remains in the superconducting state with the negative current (purple area) while switching to the normal state during the positive current (white area). The measured voltage in the superconducting state is smaller than 4×10^{-7} V (our detection limit), whereas the normal state junction voltage is 1.6 mV, meaning the diode rectification ratio demonstrated here is at least around 10^4. In addition, the switching current density and switching power are 2.2×10^2 A cm^{-2} and 12.3 nW, respectively, which are two and four orders of magnitude smaller than in the bulk superconducting diode[8].

We further probed the durability of the JD and robustness of half-wave rectification, as shown in Fig. 2b by conducting 10,000 continuous cycles with an applied square-wave excitation with an amplitude of 7.9 μA at 0.5 Hz and zero field. We note that the 'on' and 'off' state voltages stayed constant during the 10,000 cycles, and the device remains stable after that, indicating the high stability of the JD. Importantly, the JD effect is not just an ultralow temperature property; according

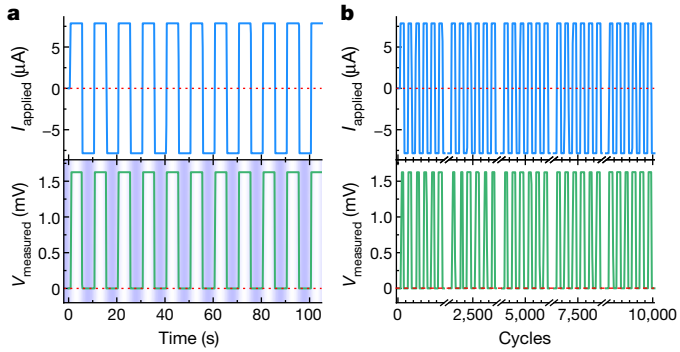

Fig. 2 | Half-wave rectification and durability test of the JD at 20 mK and zero field. a, The top panel shows the applied square-wave excitation with an amplitude of 7.9 μA (in between I_{c+} and $|I_{c-}|$) and frequency of 0.1 Hz. The bottom panel is the coincidentally measured junction voltage. The purple shaded region denotes the superconducting state in which the voltage is zero during negative current bias and the white region denotes the normal state in which the voltage is V_c during positive current bias. The red dotted line is the zero line. **b**, The top panel is the applied square-wave excitation with an amplitude of 7.9 μA and frequency of 0.5 Hz over 10,000 cycles. The bottom panel is the coincidentally measured junction voltage over those cycles, showing no degradation in the response. The red dashed lines are zero lines.

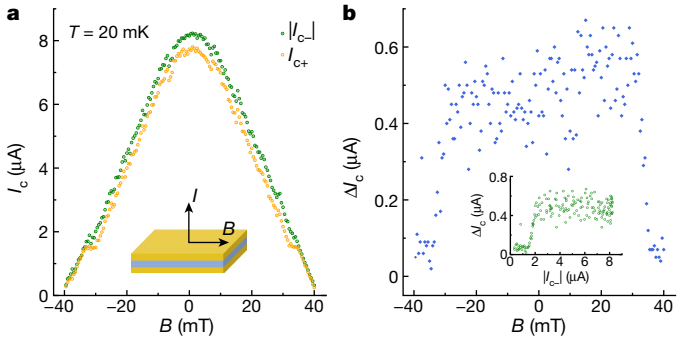

Fig. 3 | Magnetic field dependence of I_c and ΔI_c. a, I_{c+} (orange dots) and $|I_{c-}|$ (green dots) obtained from the 0–p and 0–n branches of the positive sweep as a function of applied magnetic field. The magnetic field was swept from positive to negative. The diode effect 'turns off' by ±35 mT. Inset, a schematic of the measurement geometry; the orange and blue layers represent $NbSe_2$ and Nb_3Br_8, respectively. **b**, ΔI_c as a function of magnetic field. ΔI_c is roughly field invariant until 35 mT with the diode behaviour robust in zero field. Inset, ΔI_c as a function of $|I_{c-}|$ from modulation of magnetic field with the diode effect 'turning off' below 2.1 μA.

to the asymmetric *V*–*I* curves observed at 0.9 and 3.86 K (Extended Data Fig. 2), an ideal half-wave rectification was also realized at 0.9 K whereas the half-wave rectification at 3.86 K had some punch-through error, likely due to thermal fluctuations, as shown in Extended Data Fig. 2b, d, respectively. In addition, the large hysteresis at ultralow temperatures indicates the junction is in the strongly underdamped regime. However, by 3.86 K, the p–0 (n–0) almost coincides with the 0–p (0–n) branch, indicating the junction changed to the overdamped regime (Methods), enabling possible operation frequencies of the order of the superconducting switching speed (THz)[24,33].

To further confirm the field-free nature of the JD effect, we measured *V*–*I* curves containing 0–p and 0–n branches with an in-plane magnetic field (inset of Fig. 3a) swept from 40 to −40 mT with 0.5 mT steps. As before, the I_{c+} and $|I_{c-}|$ was extracted and plotted in Fig. 3a (*V*–*I* curves with magnetic fields shown in Extended Data Fig. 3). Both I_{c+} and $|I_{c-}|$ decrease with increasing magnetic field, as expected for a JJ. Below 35 mT, ΔI_c emerges, as the $|I_{c-}|$ increases faster than I_{c+} as *B* goes to zero. Note that $|I_{c-}|$ stays larger than I_{c+} regardless of the direction of the magnetic field. Figure 3b shows the ΔI_c plotted as a function of *B*; the ΔI_c is sustained at zero field and its magnitude is independent of *B* in the low-field region. The inset of Fig. 3b shows the variation of ΔI_c with decreasing $|I_{c-}|$, and that $|I_{c-}|$ can be up to 25% larger than I_{c+}. The field-dependent ΔI_c behaviour here differs from the previously mentioned field-induced superconducting diode effect in which the ΔI_c shows an antisymmetric field dependence[8]. Also, in bulk superconductors with field-induced superconducting diode effects, ΔI_c versus *B* has been sweep direction dependent, flipping sign[8], whereas in the field-free JD demonstrated here, ΔI_c versus *B* shows no dependence on sweep direction (Extended Data Fig. 4).

To prove Josephson coupling of the junction, the d*V*/d*I* mapping as a function of bias current and magnetic field was measured and is shown in Fig. 4a. As expected, the characteristic single slit Fraunhofer pattern from the Josephson effect is observed (see Methods and Extended Data Fig. 9 for further measurements and discussion). The critical current of the JJ decreases rapidly with increasing magnetic field, consistent with the I_c decreasing in Fig. 3a. To further confirm the inversion symmetry breaking in the junction, the field-dependent first- and second-harmonic resistances were measured with an a.c. current with an amplitude of 5 μA and frequency of 7.919 Hz, as shown in Fig. 4b. The sharp drop of the first harmonic resistance in roughly ±30 mT shows the onset of superconductivity, whereas the two antisymmetric peaks appear in the second-harmonic resistance at the same fields indicating that inversion symmetry in the junction must be broken[8–10]. There can be two contributions to inversion symmetry breaking here; first is the intrinsic lack of inversion symmetry of the three-layer Nb_3Br_8, and second is the geometry of the vertical junction in which the top and bottom $NbSe_2$ electrodes are arbitrarily rotated relative to each other and the Nb_3Br_8 layer. Hence we also fabricated and measured four-layer Nb_3Br_8 devices, which show the same symmetric ΔI_c versus *B* behaviour and field-free JD effect as the three-layer Nb_3Br_8 JJ as well as antisymmetric peaks in the second-harmonic resistance measurements (see details in the Methods and Extended Data Fig. 6). These results indicate that the asymmetric $NbSe_2/Nb_3Br_8$ interfaces in the junction play an essential role for inversion symmetry breaking and the field-free JD effect.

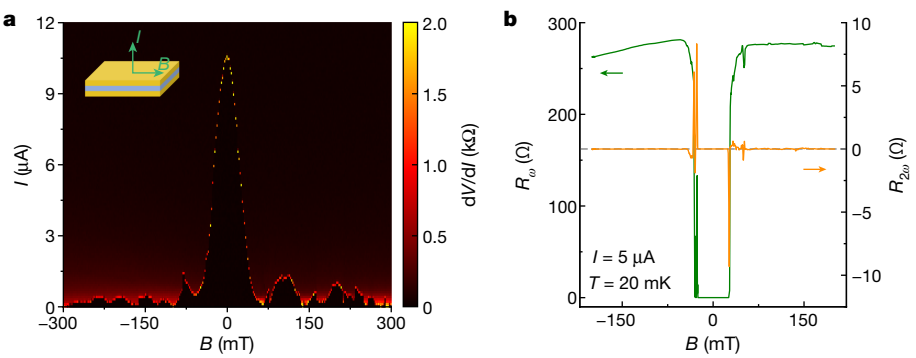

Fig. 4 | Critical current map and second-harmonic resistance of the JD. **a**, Colour map of d*V*/d*I* as a function of applied magnetic field and applied current, showing the single slit Fraunhofer pattern from the Josephson effect of a JJ. **b**, First-harmonic (green line) and second-harmonic (orange line) resistances measured by applying an a.c. current of 5 μA at 20 mK. The antisymmetric peaks in the second harmonic correspond with the critical field, showcasing the non-reciprocal nature of the superconductivity.

Discussion

We discuss the possible origin of ΔI_c and the diode behaviour. Fundamentally, to obtain a ΔI_c and ΔI_r, an asymmetric V–I curve is required, that is, the I_+ behaviour needs to be distinct from the I_- behaviour. From the phenomenological resistively and capacitively shunted junction (RCSJ) model of a JJ[17], the total current through the junction I is determined by $I = I_F + I_{Cap} + I_R + I_J$, where I_F is the fluctuation current of the noise channel, I_{Cap} is the current of the capacitive channel, I_R is the extra resistive channel arising from finite temperature quasiparticle excitation and I_J is the Josephson current. As I_F, I_{Cap} and I_R have negligible influence on the critical current (see the Methods for details), we speculate that the critical current through the JJ should be governed by the Josephson current I_J, ($I_J = I_c \sin\varphi$, where φ is phase difference of two superconductors). Because ΔI_c is suppressed with B and I_{c+} (I_{c-}) are symmetric with B, and the current is parallel to the symmetry breaking direction while perpendicular to magnetic field direction in our junction, magnetochiral anisotropy can be ruled out as the driving mechanism here. Also to exclude the $NbSe_2$ electrodes as the driving factor, we fabricated JJs of arbitrarily rotated $NbSe_2/NbSe_2$ and $NbSe_2$/few-layer graphene (FLG)/$NbSe_2$ junctions[34,35], and found they both show a field-induced superconducting diode effect with antisymmetric ΔI_c versus B characteristics (Methods and Extended Data Figs. 7 and 8). Therefore, in the Nb_3Br_8 JJs, ΔI_c must be induced by asymmetric Josephson tunnelling at a zero field.

Recently, Kitamura et al. discussed non-reciprocal Landau–Zener tunnelling in inversion symmetry breaking materials with polarization[36], explaining that the effect in the normal state originates from direction dependent modulation of the electron tunnelling probability across a tunnel barrier because of a shift in wave-packet position. Alternatively, Hu et al. proposed a JD based on an interface of p- and n-doped superconductors[2] that breaks inversion symmetry and forms a polarized Mott-insulating region that can be suppressed by voltage in one direction and elongated in the other direction, resulting in diodic behaviour.

In the situation of $NbSe_2/Nb_3Br_8/NbSe_2$ JJs, Nb_3Br_8 was recently predicted to be an obstructed atomic insulator (OAI) with Wannier charge centres symmetrically pinned at the unoccupied inversion centres in between two Br-Nb-Br layers[37,38] (Methods and Extended Data Fig. 10). The negative charge centres are separated from the positive ones along the c axis of the crystal, and combined with the asymmetric $NbSe_2/Nb_3Br_8$ interfaces, an out-of-plane (OOP) polarization can occur[38]. In analogy to the previously described theoretical works of polarized systems, we propose that a polarization in the $NbSe_2/Nb_3Br_8/NbSe_2$ JJs may induce asymmetric Josephson tunnelling and lead to the field-free JD effect; further theoretical and experimental study is necessary to fully explain the mechanism.

Also, future optimization of the JD architecture through tuning the geometry or type of barrier can result in more ideal diodic behaviour. Creating further quantum material JJs, such as those demonstrated here, can uncover emergent phenomena leading to new or anomalous Josephson phenomena through the effect of the intrinsic properties of the barrier. Future work combining materials possessing properties such as topological states, ferroelectricity, magnetoelectricity, non-collinear magnetism, OAI and emergent properties from twisted heterostructures, with superconducting electrodes may allow the realization of new Josephson phenomena. Thus the opportunities for creating superconducting electronics using quantum materials are vast and just beginning.

Online content

Any methods, additional references, Nature Research reporting summaries, source data, extended data, supplementary information, acknowledgements, peer review information; details of author contributions and competing interests; and statements of data and code availability are available at https://doi.org/10.1038/s41586-022-04504-8.

1. Misaki, K. & Nagaosa, N. Theory of the nonreciprocal Josephson effect. *Phys. Rev. B* **103**, 245302 (2021).
2. Hu, J., Wu, C. & Dai, X. Proposed design of a Josephson diode. *Phys. Rev. Lett.* **99**, 067004 (2007).
3. Chen, C.-Z. et al. Asymmetric Josephson effect in inversion symmetry breaking topological materials. *Phys. Rev. B* **98**, 075430 (2018).
4. Tokura, Y. & Nagaosa, N. Non-reciprocal responses from non-centrosymmetric quantum materials. *Nat. Commun.* **9**, 3740 (2018).
5. Fruchart, M., Hanai, R., Littlewood, P. B. & Vitelli, V. Non-reciprocal phase transitions. *Nature* **592**, 363–369 (2021).
6. Akamatsu, T. et al. A van der Waals interface that creates in-plane polarization and a spontaneous photovoltaic effect. *Science* **372**, 68–72 (2021).
7. Sze, S. M. & Lee, M.-K. *Semiconductor Devices: Physics and Technology* 3rd edn (Wiley, 2012).
8. Ando, F. et al. Observation of superconducting diode effect. *Nature* **584**, 373–376 (2020).
9. Wakatsuki, R. et al. Non-reciprocal charge transport in noncentrosymmetric superconductors. *Sci. Adv.* **3**, e1602390 (2017).
10. Zhang, E. et al. Nonreciprocal superconducting $NbSe_2$ antenna. *Nat. Commun.* **11**, 5634 (2020).
11. Baumgartner, C. et al. Supercurrent rectification and magnetochiral effects in symmetric Josephson junctions. *Nat. Nanotechnol.* **17**, 39–44 (2022).
12. Yuan, N. F. Q. & Fu, L. Supercurrent diode effect and finite momentum superconductivity. Preprint at https://arxiv.org/abs/2106.01909 (2021).
13. Daido, A., Ikeda, Y. & Yanase, Y. Intrinsic superconducting diode effect. *Phys. Rev. Lett.* **128**, 037001 (2022).
14. Ideue, T. et al. Bulk rectification effect in a polar semiconductor. *Nat. Phys.* **13**, 578–583 (2017).
15. Ideue, T., Koshikawa, S., Namiki, H., Sasagawa, T. & Iwasa, Y. Giant nonreciprocal magnetotransport in bulk trigonal superconductor $PbTaSe_2$. *Phys. Rev. Res.* **2**, 042046(R) (2020).
16. Wang, Y. et al. Gigantic magnetochiral anisotropy in the topological semimetal $ZrTe_5$. Preprint at https://arxiv.org/abs/2011.03329 (2021).
17. Likharev, K. K. *Dynamics of Josephson Junctions and Circuits* (Gordon and Breach Science Publishers, 1986).
18. Likharev, K. K. Superconducting weak links. *Rev. Mod. Phys.* **51**, 101–159 (1979).
19. Dubos, P. et al. Josephson critical current in a long mesoscopic S-N-S junction. *Phys. Rev. B* **63**, 064502 (2001).
20. Golubov, A. A., Kupriyanov, M. Y. & Il'ichev, E. The current-phase relation in Josephson junctions. *Rev. Mod. Phys.* **76**, 411–469 (2004).
21. Lee, G.-H. et al. Graphene-based Josephson junction microwave bolometer. *Nature* **586**, 42–46 (2020).
22. Walsh, E. D. et al. Josephson junction infrared single-photon detector. *Science* **372**, 409–412 (2021).
23. Clarke, J. & Wilhelm, F. K. Superconducting quantum bits. *Nature* **453**, 1031–1042 (2008).
24. Likharev, K. K. & Semenov, V. K. RSFQ logic/memory family: a new Josephson-junction technology for sub-terahertz-clock-frequency digital systems. *IEEE Trans. Appl. Supercond.* **1**, 3–28 (1991).
25. Devoret, M. H. & Schoelkopf, R. J. Superconducting circuits for quantum information: an outlook. *Science* **339**, 1169–1174 (2013).
26. Jiang, J. et al. Exploration of new ferromagnetic, semiconducting and biocompatible Nb_3X_8 (X = Cl, Br or I) monolayers with considerable visible and infrared light absorption. *Nanoscale* **9**, 2992–3001 (2017).
27. Pasco, C. M., El Baggari, I., Bianco, E., Kourkoutis, L. F. & McQueen, T. M. Tunable magnetic transition to a singlet ground state in a 2D van der Waals layered trimerized Kagome magnet. *ACS Nano* **13**, 9457–9463 (2019).
28. Yoon, J. et al. Anomalous thickness-dependent electrical conductivity in van der Waals layered transition metal halide, Nb_3Cl_8. *J. Phys. Condens. Matter* **32**, 304004 (2020).
29. Haraguchi, Y. et al. Magnetic-nonmagnetic phase transition with interlayer charge disproportionation of Nb_3 trimers in the cluster compound Nb_3Cl_8. *Inorg. Chem.* **56**, 3483–3488 (2017).
30. Sheckelton, J. P., Plumb, K. W., Trump, B. A., Broholm, C. L. & McQueen, T. M. Rearrangement of van der Waals stacking and formation of a singlet state at T = 90 K in a cluster magnet. *Inorg. Chem. Front.* **4**, 481–490 (2017).
31. Castellanos-Gomez, A. et al. Deterministic transfer of two-dimensional materials by all-dry viscoelastic stamping. *2D Mater.* **1**, 011002 (2014).
32. Xi, X. et al. Ising pairing in superconducting $NbSe_2$ atomic layers. *Nat. Phys.* **12**, 139–143 (2015).
33. Kleiner, R., Koelle, D., Ludwig, F. & Clarke, J. Superconducting quantum interference devices: state of the art and applications. *Proc. IEEE* **92**, 1534–1548 (2004).
34. Yabuki, N. et al. Supercurrent in van der Waals Josephson junction. *Nat. Commun.* **7**, 10616 (2016).
35. Kim, M. et al. Strong proximity Josephson coupling in vertically stacked $NbSe_2$-graphene-$NbSe_2$ van der Waals junctions. *Nano Lett.* **17**, 6125–6130 (2017).
36. Kitamura, S., Nagaosa, N. & Morimoto, T. Nonreciprocal Landau–Zener tunneling. *Commun. Phys.* **3**, 63 (2020).
37. Xu, Y. et al. Filling-enforced obstructed atomic insulators. Preprint at https://arxiv.org/abs/2106.10276 (2021).
38. Xu, Y. et al. Three-dimensional real space invariants, obstructed atomic insulators and a new principle for active catalytic sites. Preprint at https://arxiv.org/abs/2111.02433 (2021).

Methods

Synthesis of Nb_3Br_8 crystal

Nb_3Br_8 crystals used in this work were grown through chemical vapour transport. Stoichiometric mixtures of niobium powder (Alfa, 99.99%) and $NbBr_5$ (Strem, 99.9%) with a total mass of 1.5 g were ground together and added to a 14 mm inner diameter (with a 2 mm thick wall) fused silica tube in a glovebox and handled using standard air free techniques. Next, 20 mg of NH_4Br was included as a transport agent. The tubes were then sealed air free at a length of approximately 30 cm, about 5 cm longer than the first two zones of a three-zone furnace. A three-zone furnace was used with a temperature gradient of 840, 785 and 795 °C with all but the last few centimetres of the tube between the first two zones. This discouraged the formation of large intergrown clumps of crystals at the end of the tube. The furnace was held at temperature for 3–5 days before being cooled to room temperature over 7 h.

Fabrications of the JJ device

We fabricated the $NbSe_2/Nb_3Br_8/NbSe_2$ JJ in a glove box with an inert environment to avoid oxidation and decay. The bottom $NbSe_2$ flake was directly exfoliated from an $NbSe_2$ single crystal (HQ graphene) to a SiO_2/Si wafer, then Nb_3Br_8 thin film and top $NbSe_2$ flake were exfoliated and successively transferred layer by layer by using the polydimethylsiloxane assistant dry transfer method[31]. A h-BN (HQ graphene) layer was finally transferred on the top to protect the JJ from degradation in the atmosphere. Then Ti (3 nm)/Au (50 nm) electrodes were deposited on the top and bottom $NbSe_2$ flakes for transport measurement.

Transport measurements

The transport properties of JJ device were measured in a BlueFors dilution refrigerator with a base temperature of 20 mK. A Keithley 6221 AC/DC Current Source Meter was used to inject both d.c. current and square-wave excitation, and the d.c. voltage was measured using a Keithley 2182a Nanovoltmeter. The a.c. measurements were performed by injecting a.c. current with a frequency of ω (7.919 Hz) using a Zurich MFLI amplifier, and the second-harmonic signals were obtained from the out-of-phase 2ω component of the a.c. voltage. A Fraunhofer pattern was obtained by measuring the differential resistance (dV/dI) versus I curve under different magnetic fields using a lock-in amplifier (Zurich MFLI) with a d.c. bias (Keithley 2636).

Excluding the Joule heating effect

In Fig. 1b, we measured positive and negative sweep V–I curves with the same sweep rates. These two curves lie on top of each other, indicating that the V–I curves and associated I_{c+} and I_{c-} are not dependent on the two sweep directions. As shown in Fig. 1c, the V–I is asymmetric and I_{c+} and I_{c-} have prominently different values. In general, the Joule heating effect is proportional to the heating time and the I_{c+} (or I_{c-}) obtained in positive and negative sweeps undergo different heating times, which can cause different local temperatures in sample. If the asymmetric V–I was induced by the Joule heating effect, the values of I_{c+} and $|I_{c-}|$ would switch for the positive and negative sweeps: that is, the effect would be sweep direction dependent. However, the V–I curves of positive and negative sweeps are the same, strongly indicating that the different I_{c+} and I_{c-} obtained indeed are intrinsic to the device rather than induced extrinsically by the Joule heating effect.

Magnetoresistance characterization of Nb_3Br_8 thin flake

The Nb_3Br_8 single crystal has previously been shown to have a phase transition from a high temperature ferromagnetic state to a magnetic singlet ground state at low temperatures (β phase)[27]. Here we use transport measurements to investigate the magnetic property of a Nb_3Br_8 thin flake. First, we measured sweep-up (magnetic field sweep from negative to positive) and sweep-down (magnetic field sweep from positive to negative) magnetoresistances of $NbSe_2/Nb_3Br_8/NbSe_2$ JJ (device 1, device in main text) with a temperature above T_c of $NbSe_2$ superconducting electrodes. Extended Data Fig. 5a, b shows the magnetoresistances of device 1 at 10 K with in-plane and OOP magnetic fields up to 7 T, respectively. The overlapping sweep-up and sweep-down magnetoresistances curves reveal no hysteresis or reversion between these curves, indicating no ferromagnetic signal in the Nb_3Br_8 thin flakes[39,40]. Moreover, we also replaced $NbSe_2$ superconducting electrodes with FLG to fabricate FLG/Nb_3Br_8/FLG devices and measured their magnetoresistances with an OOP magnetic field. Extended Data Fig. 5c shows the results of one of the FLG/Nb_3Br_8/FLG devices (device 6) measured at 2 K. Similar to the results in device 1, the magnetoresistances overlap well and no hysteresis or reversion signals can be observed in the curves, which is also consistent with the observation of the magnetic singlet ground state[27]. It is worth noting that the oscillations in FLG/Nb_3Br_8/FLG device are induced by the quantum oscillation of FLG.

Field-free JD effect in a $NbSe_2$/four-layer $Nb_3Br_8/NbSe_2$ JJ (device 3)

A $NbSe_2/Nb_3Br_8/NbSe_2$ JJ with a four-layer Nb_3Br_8 as the tunnel barrier (device 3) was fabricated using the same technique as device 1 (device in main text). We measured V–I curves at different magnetic fields at 20 mK, and extracted I_{c+} and $|I_{c-}|$ from 0–p and 0–n branches, respectively, and plotted them as a function of magnetic field as shown in Extended Data Fig. 6a. The I_{c+} and $|I_{c-}|$ show similar tendencies and behaviours to device 1. Extended Data Fig. 6b shows the field-dependent calculated ΔI_c. The non-zero ΔI_c can be clearly observed at zero field and low-field region, and it decreases to almost zero at relative higher fields, which is similar to the phenomenon in device 1. Therefore, the JJ with four-layer Nb_3Br_8 also has a field-free JD effect. To confirm the inversion symmetry breaking, we also performed the second-harmonic resistances ($R_{2\omega}$) measurements at 20 mK with an applied current of 4 μA, as shown in Extended Data Fig. 6c. The two antisymmetric $R_{2\omega}$ peaks corresponding with the superconducting transition of R_ω reveal the inversion symmetry breaking nature of the JJ[9,15]. Because the four-layer Nb_3Br_8 preserves inversion symmetry, as shown in Extended Data Fig. 1a, the inversion symmetry breaking of device 3 originates from the different interfaces of the top and bottom $NbSe_2/Nb_3Br_8$.

Magnetic-field-induced superconducting diode effects in $NbSe_2/NbSe_2$ (devices 4 and 7) and $NbSe_2$/FLG/$NbSe_2$ (device 5) junctions

We also fabricated other junctions as control experiments to narrow the suspects of the field-free JD effect mechanism. First, we considered the influence of the superconducting electrode $NbSe_2$, which is a type II and multi-gapped superconductor. A previous study reported non-reciprocal transport in atomically thin $NbSe_2$ films that broke inversion symmetry, which disappeared in bulk $NbSe_2$ crystal[10]. In all our devices, we used thick $NbSe_2$ flakes (>20 nm) as superconducting electrodes, which have similar properties to bulk $NbSe_2$. We also fabricated a $NbSe_2/NbSe_2$ junction (device 4) to explore its property. Extended Data Fig. 7a shows the V–I curve measured with the positive sweep (a sequence of 0–p, p–0, 0–n and n–0 branches) at 2 K and 0 T. As shown in Extended Data Fig. 7a, there are three transition steps in the V–I curve, which correspond with the critical currents of junction, bottom and top $NbSe_2$ electrodes, respectively. There is no obvious difference between I_{c+} and I_{c-} of the junction. The field dependence of critical currents was further measured; we extracted the I_{c+} and $|I_{c-}|$ of the junction from each V–I curve measured at different magnetic fields and plotted them as a function of magnetic field as shown in Extended Data Fig. 7b. The I_{c+} and $|I_{c-}|$ seemed to have a mirror symmetry with each other. ΔI_c was also calculated and is shown in Extended Data Fig. 7c. The antisymmetric ΔI_c curve indicates that a $NbSe_2/NbSe_2$ junction can only show a field-induced superconducting diode effect, rather than a field-free JD effect observed in $NbSe_2/Nb_3Br_8/NbSe_2$ junctions. Second, to further confirm the influence of barrier materials, we also fabricated a $NbSe_2$/FLG/$NbSe_2$ junction (device 5) as a control experiment. The I_{c+}

and $|I_{c-}|$ was extracted as before and shown in the inset of Extended Data Fig. 7d. ΔI_c was also calculated and plotted as a function of magnetic field in Extended Data Fig. 7d. Similar to the results from the $NbSe_2$/$NbSe_2$ junction device (device 4), the $NbSe_2$/FLG/$NbSe_2$ junction also shows the field-induced superconducting diode effect.

Previous studies have shown that a self-field effect in tunnel junctions with a large critical current density can result in a skewed Fraunhofer pattern, which may contribute to the field-induced superconducting diode effect in these junctions[41,42]. We also fabricated a $NbSe_2$/$NbSe_2$ control device (device 7) with low critical current ($I_c \cong 120$ μA) and a correspondingly lower critical current density ($J_c \cong 18.5$ μA μm^{-2}) than device 4, $J_c \cong 66$ μA μm^{-2}. Extended Data Fig. 8 shows the I_c and corresponding ΔI_c as a function of applied magnetic field. The I_{c+} and $|I_{c-}|$ versus B have a mirror symmetry with each other, and the obvious antisymmetric feature of ΔI_c versus B curve also confirms the field-induced superconducting diode effect in device 7, similar to device 4.

In addition, recent studies on planar Nb/WTe_2/Nb JJs[43] and the indium arsenide two-dimensional electron gas system[11], in which the self-field effect does not exist, also reported a mirrored I_{c+} ($|I_{c-}|$) versus B curves, similar to the results from these $NbSe_2$/$NbSe_2$ and $NbSe_2$/FLG/$NbSe_2$ junctions. So far, the field-induced superconducting diode effect has been proposed to arise from effects such as magnetochiral anisotropy[9], finite momentum superconductivity[12] and non-reciprocal Landau critical momentum[13]. More investigation is needed to understand the origin of field-induced diode effect in $NbSe_2$/$NbSe_2$ and $NbSe_2$/FLG/$NbSe_2$ junctions.

In summary, both $NbSe_2$/$NbSe_2$ and $NbSe_2$/FLG/$NbSe_2$ junctions show the field-induced superconducting diode effect, similar to the behaviour of the $[Nb/V/Ta]_n$ superlattice[8]. These observations in $NbSe_2$/$NbSe_2$ and $NbSe_2$/FLG/$NbSe_2$ junctions indicate that the field-free JD effect does not originate from the superconducting property of $NbSe_2$. Also, even though the interfaces of these junctions also break the inversion symmetry, the field-free JD effect dose not occur. These results, along with the observations in $NbSe_2$/Nb_3Br_8/$NbSe_2$ devices (devices 1 and 3), indicate that the field-free JD effect originates from asymmetric Josephson tunnelling induced by the Nb_3Br_8 barrier and the associated $NbSe_2$/Nb_3Br_8 interfaces in the junction.

Basic analysis of the JJ (device 1) and discussion of Fraunhofer patterns (devices 1 and 2)

The large hysteresis between 0–p (0–n) and p–0 (n–0) branches on the V–I curves (Fig. 1b) indicates the JJ (device 1) lies in the underdamped region. On the basis of the critical current (I_c) and return current (I_r) of V–I curve measured at 20 mK, the Stewart–McCumber parameter ($\beta_c \cong \left(\frac{4I_c}{\pi I_r}\right)^2$) $NbSe_2$/Nb_3Br_8/$NbSe_2$ JJ is 21, which is much larger than 1, further confirming that the JJ is in underdamped region[17,18]. On the basis of the equation $\beta_c = \frac{2e}{\hbar} I_c R_N^2 C$ (where C is the capacitance and R_N is normal state resistance of junction)[17,18], the junction capacitance calculated is 2.0×10^{-14} F, corresponding with specific capacitance (C/A, where A is the junction area and is roughly 3.68 μm^2 in device 1) of 0.54 μF cm^{-2}.

The Fraunhofer pattern in Fig. 4a is measured with a sweep-up magnetic field and Extended Data Fig. 9a shows the Fraunhofer pattern measured with a sweep-down magnetic field, which is similar to the sweep-up one. Both Fraunhofer patterns are not so periodic at higher field, which is a common case as seen in many other two-dimensionaltunnel JJs, including $NbSe_2$/$NbSe_2$ junctions[34] as well as $NbSe_2$/graphene/$NbSe_2$ junctions[35]. In these vertical junctions with very thin barriers, the Fraunhofer pattern can be influenced by many effects, such as magnetic vortices in the superconducting electrodes and the self-field effect[35], which can make it difficult to get an ideal, highly periodic Fraunhofer pattern. In addition, from the theory, the ideal Fraunhofer pattern requires a uniform current profile (rectangular junction area shape and magnetic field parallel with either side of the rectangle). Therefore, the junction shape and magnetic field direction can also lead to a non-ideal Fraunhofer pattern, even in a high-quality junction with high-quality interfaces[44].

Here we also characterized more junction parameters by analysing the Fraunhofer pattern in Extended Data Fig. 9a at a low magnetic field. In a JJ, the London penetration depth (λ) of $NbSe_2$ can be obtained from $\phi_0 = \Delta B W (d + 2\lambda)$, where ϕ_0 is the magnetic flux quantum, ΔB is the period of the oscillation in the Fraunhofer, W is the width of the junction perpendicular to the field direction and d is the barrier thickness. From the Fraunhofer pattern, the oscillation period is roughly 59 mT and with $W \cong 3.5$ μm and $d \cong 2.3$ nm, λ is calculated to be 3.85 nm.

In addition, to further demonstrate the $NbSe_2$/Nb_3Br_8/$NbSe_2$ heterostructure is indeed a JJ, we fabricated another $NbSe_2$/2-layer Nb_3Br_8/$NbSe_2$ heterostructure device (device 2), and obtained the expected high-quality Fraunhofer pattern, as shown in Extended Data Fig. 9b. Moreover, the field-free JD effect is also observed in this junction, as shown in Extended Data Fig. 9c and its inset. The $|I_c|$ and $|I_{c-}|$ versus B curves shown in the inset of Extended Data Fig. 9c show a similar tendency and behaviour to device 1, and the extracted ΔI_c shows non-zero values at zero field and in the low-field region, and decreases to around zero at higher fields similar to device 1.

Discussion on RCSJ mode of JD

Here we discuss field-free JD behaviour based on the phenomenological RCSJ model of a JJ[17]; the total current through the junction I is determined by $I = I_F + I_{Cap} + I_R + I_J$, where I_F is the fluctuation current of the noise channel, I_{Cap} is the current of the capacitive channel, I_R is the extra resistive channel arising from finite temperature quasiparticle excitation and I_J is the Josephson current. In d.c. measurement, the thermal noise current (I_T) dominates the fluctuation current, which can be calculated according to equation $I_T = (2e/\hbar)k_B T$ (ref. [17]), where $\hbar$ is reduced Planck constant, k_B is Boltzmann constant, e is elementary charge and T is the temperature. At 20 mK, I_T is about 0.8 nA, far less than ΔI_c, and so will be disregarded as a cause of the V–I asymmetry. In principle, the other three components could have asymmetric V–I responses if inversion/time reversal symmetry is broken. Below, we examine each of those possibilities in the context of our JJ.

Regarding the capacitive channel, as mentioned earlier, Misaki et al.[1] proposed that in an inversion symmetry broken JJ, an asymmetric charging energy of capacitance can lead to a ΔI_r, without an applied magnetic field, which was observed in our JJ device (Fig. 1c). However, this model did not include an expectation of a ΔI_c, which is one of the main requirements (the other being sharp transitions) for realizing half-wave rectification. As I_r corresponds with the return to the superconducting state, applying a square-wave current excitation with an amplitude of $I_{r+} + \Delta I_r/2$, for example, would not result in rectification as both ends of the wave lie in the superconducting regime.

Considering the extra resistive channel ($I_R = V/R_N$) from quasiparticle excitations, its contribution to the diode effect would stem from asymmetry in R_N and be significant if the resistance in the superconducting state was not zero. However, because the voltage in the superconducting state is zero in our device, the contribution of I_R to the critical current can be neglected. Therefore, the critical current through the JJ is governed by the Josephson current I_J, ($I_J = I_c \sin\varphi$, $I_c = V_o/R_N$ and φ is phase difference of two superconductors). The difference of positive and negative critical currents should originate from the asymmetric Josephson tunnelling in our JJ.

The OAI phase of Nb_3Br_8

The crystal structure of Nb_3Br_8 has the symmetries of the space group 166 ($R\bar{3}m$), as shown in Extended Data Fig. 1a, in which Nb and Br atoms occupy the Wyckoff positions 6c and 18h, respectively. The electronic band structure and the band representation analysis of Nb_3Br_8 have been studied[38,45], and the symmetry properties of its valence bands can be characterized by the multiplicities of irreducible representations at all the high-symmetry momenta, which is referred to as the symmetry data vector,

$$B = (m(\bar{\Gamma}_4\bar{\Gamma}_5), m(\bar{\Gamma}_6\bar{\Gamma}_7), m(\bar{\Gamma}_8), m(\bar{\Gamma}_9), m(\bar{\Gamma}_3\bar{\Gamma}_4), m(\bar{\Gamma}_5\bar{\Gamma}_6), \ldots, m(\bar{\Gamma}_9))^T = (15, 15, 33, 32, 48, 47, 47, 48, 15, 15, 32, 33)^T \quad (1)$$

where $m(\rho)$ represents the multiplicity of the irreducible representations ρ formed by the occupied Bloch bands at the corresponding high-symmetry momentum. From topological quantum chemistry[46], the band representation, which are characterized by the above symmetry data vector, can be expressed as a linear combination of several elementary band representations (which are the band representations induced from atomic orbitals) with non-negative-integer coefficients. Hence, Nb_3Br_8 is a topologically trivial insulator.

A topologically trivial insulator can be further classified as an atomic insulator or an OAI. If the band representation of a topological insulator cannot be induced from only the atomic orbitals at atom occupying sites, there must be some atomic orbitals (or Wannier functions) centred at the empty sites (that is, the Wyckoff positions that are not occupied by any atoms) and this topologically trivial insulator is referred to as OAI. The OAIs can be indicated by the non-zero integer real space invariants at the empty sites and all the OAIs on the Topological materials database (https://www.topologicalquantumchemistry.org)[46] have been exhausted by performing a high-throughput calculations[38], in which Nb_3Br_8 is identified as an OAI material indicated by a non-zero real space invariants at the empty Wyckoff position 3b, whose definition is

$$\delta(b) = \frac{1}{2}[-m(\bar{\Gamma}_6\bar{\Gamma}_7) + m(\bar{\Gamma}_9) + m(\bar{F}_5\bar{F}_6) - m(\bar{L}_5\bar{L}_6) + m(\bar{T}_6\bar{T}_7) - m(\bar{T}_9)]. \quad (2)$$

By substituting the symmetry data vector in equation (1) in to equation (2), we have $\delta(b) = -1$, which means there must have a Wannier function centred at 3b. As the positions of 3b is not occupied by any atom, $\delta(b) = -1$indicates that Nb_3Br_8 is an OAI and the Wyckoff position 3b is referred to as the obstructed Wannier charge centre.

To demonstrate the OAI phase of Nb_3Br_8, we have also calculated the electron density distribution in the lattice of Nb_3Br_8. As the results show in Extended Data Fig. 10, the electron charge density is symmetrically centred at the Wyckoff position 3b (the inversion centre between two Nb_3Br_8 layers), indicating the special separation of positive and negative charge centres along the *c* axis of the crystal. In the heterostructures of $NbSe_2/Nb_3Br_8/NbSe_2$, the asymmetric top and bottom interfaces break inversion symmetry of the whole junction along *c* axis. The distribution of charge centres between layers is easy to be influenced by this symmetry breaking, which could result in the charge polarization in the whole junction along *z* direction and hence show an OOP polarization. As discussed in the main text, in analogy to previous theoretical investigations of the polarized system[2,36], we propose that a polarization in the $NbSe_2/Nb_3Br_8/NbSe_2$ JJs may induce asymmetric Josephson tunnelling and lead to the field-free JD effect; further theoretical and experimental study is necessary to fully explain the mechanism.

Data availability

The data that support the findings of this study are available from the corresponding authors upon reasonable request.

39. Song, T. et al. Giant tunneling magnetoresistance in spin-filter van der Waals heterostructures. *Science* **360**, 1214–1218 (2018).
40. Wang, Z. et al. Very large tunneling magnetoresistance in layered magnetic semiconductor CrI_3. *Nat. Commun.* **9**, 2516 (2018).
41. Krasnov, V. M., Oboznov, V. A. & Pedersen, N. F. Fluxon dynamics in long Josephson junctions in the presence of a temperature gradient or spatial nonuniformity. *Phys. Rev. B* **55**, 14486–14498 (1997).
42. Goldman, A. M. & Kreisman, P. J. Meissner effect and vortex penetration in Josephson junctions. *Phys. Rev.* **164**, 544–547 (1967).
43. Kononov, A. et al. One-dimensional edge transport in few-layer WTe_2. *Nano Lett.* **20**, 4228–4233 (2020).
44. Watanabe, N. et al. The shape dependency of two-dimensional magnetic field dependence of a Josephson junction. *J. Appl. Phys.* **103**, 07C707 (2008).
45. Vergniory, M. G. et al. A complete catalogue of high-quality topological materials. *Nature* **566**, 480–485 (2019).
46. Bradlyn, B. et al. Topological quantum chemistry. *Nature* **547**, 298–305 (2017).

Acknowledgements We thank J. Song, G.-H. Lee and Y. Wang for valuable discussions. We thank P. Wang for support during preparation of Fig. 1a. M.N.A. acknowledges that this research was principally supported by the Alexander von Humboldt Foundation Sofia Kovalevskaja Award, the German Federal Ministry of Education and Research's MINERVA ARCHES Award, the Max Planck Society and Delft University of Technology. Y.-J.Z. acknowledges the Shenzhen Science and Technology Project under grant no. JCYJ20180507182246321. S.S.P.P. acknowledges the European Research Council under the European Union's Horizon 2020 research and innovation programme (grant agreement no. 670166), Deutsche Forschungsgemeinschaft (DFG, German Research Foundation)—project number 314790414 and Alexander von Humboldt Foundation in the framework of the Alexander von Humboldt Professorship endowed by the Federal Ministry of Education and Research. T.M. acknowledges the David and Lucile Packard Foundation and the Johns Hopkins University Catalyst Award.

Author contributions H.W. and M.N.A. conceived and designed the study. C.P. grew the samples. H.W. and Y.W. fabricated the devices. H.W., Y.W., P.K.S. and U.F. performed the transport measurements. H.W. and Y.W. carried out the data analysis. Y.X. provided theoretical support and discussion. Y.-J.Z. and S.S.P.P. provided facility and instrument support. T.M. and M.N.A. are the principal investigators. All authors contributed to the preparation of the manuscript.

Competing interests The authors declare no competing interests.

Additional information

Supplementary information The online version contains supplementary material available at https://doi.org/10.1038/s41586-022-04504-8.

Correspondence and requests for materials should be addressed to Heng Wu or Mazhar N. Ali.

Peer review information *Nature* thanks Kanda Akinobu and the other, anonymous, reviewer(s) for their contribution to the peer review of this work. Peer reviewer reports are available.

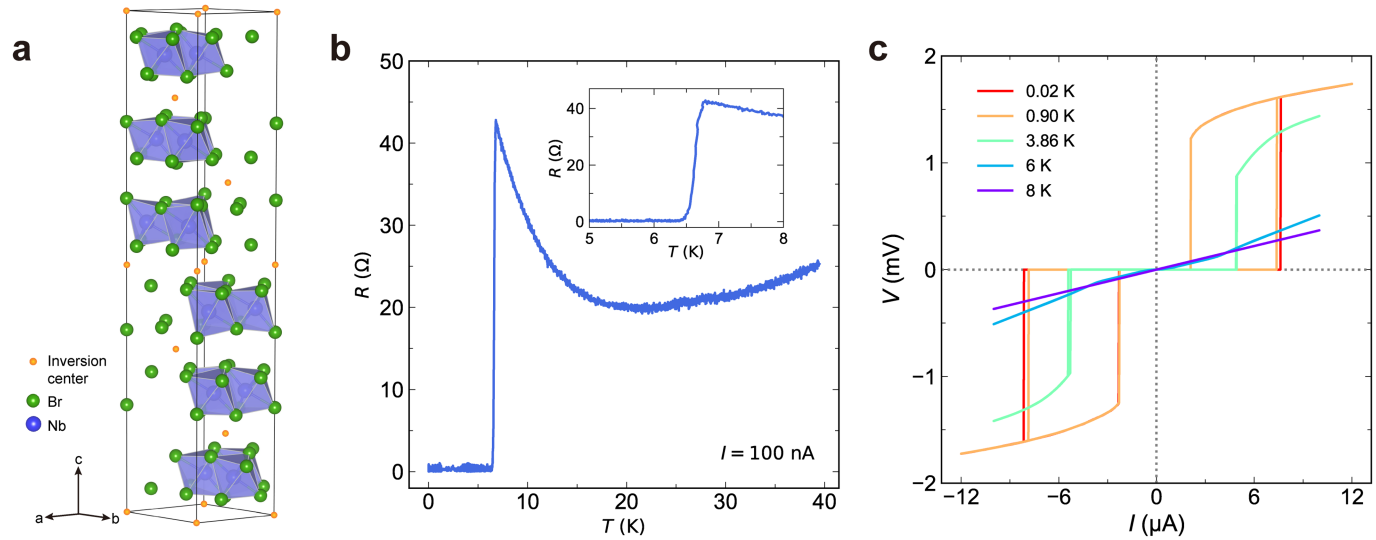

Extended Data Fig. 1 | Temperature dependent resistance and *V-I* curves of the Josephson diode. a, Nb_3Br_8: crystal structure and inversion center locations. **b**, Resistance versus temperature measured using an a.c. current of 100 nA. Inset shows the enlarged plot near the superconducting transition of 6.6 K. **c**, *V-I* curves with positive sweep measured at different temperatures showing nonlinear behavior appearing below T_c.

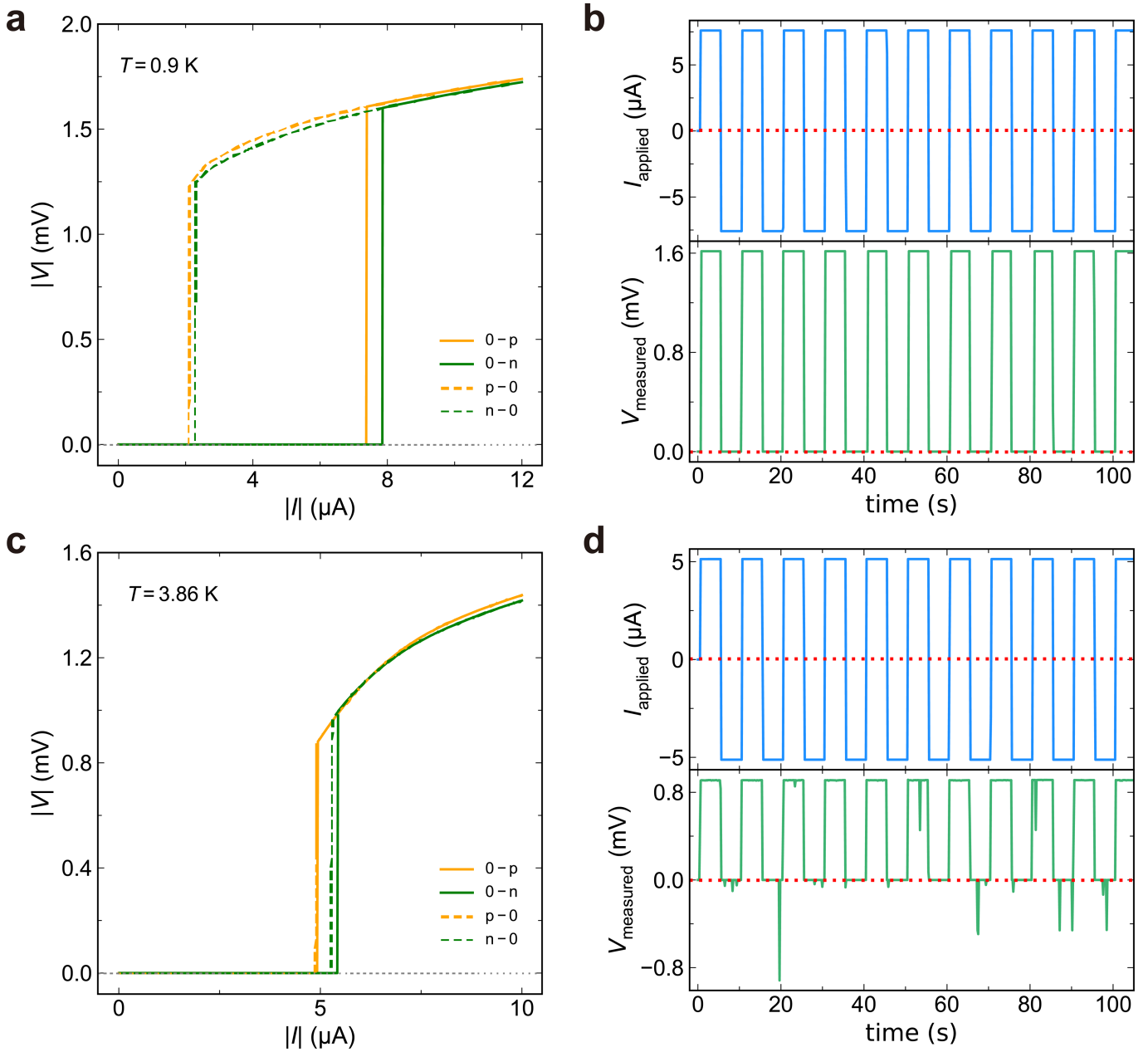

Extended Data Fig. 2 | *V-I* curves and half-wave rectification at different temperatures. a, Positive sweep *V-I* curve measured at 0.9 K. Both ΔI_c and ΔI_r are visible. **b**, Half-wave rectification measured at 0.9 K with an applied current of 7.6 μA at 0.1 Hz. The red dotted lines are the zero lines, showing that junction is in the superconducting state with negative current and switches to the normal state with positive current. **c**, Positive sweep *V-I* curve measured at 3.86 K. ΔI_c is still visible, while the hysteresis is almost completely suppressed. **d**, Half-wave rectification measured at 3.86 K with an applied current of 5.14 μA at 0.1 Hz. The red dotted lines are the zero lines. Imperfect rectification is evident with some punch-through error, probably due to thermal fluctuation.

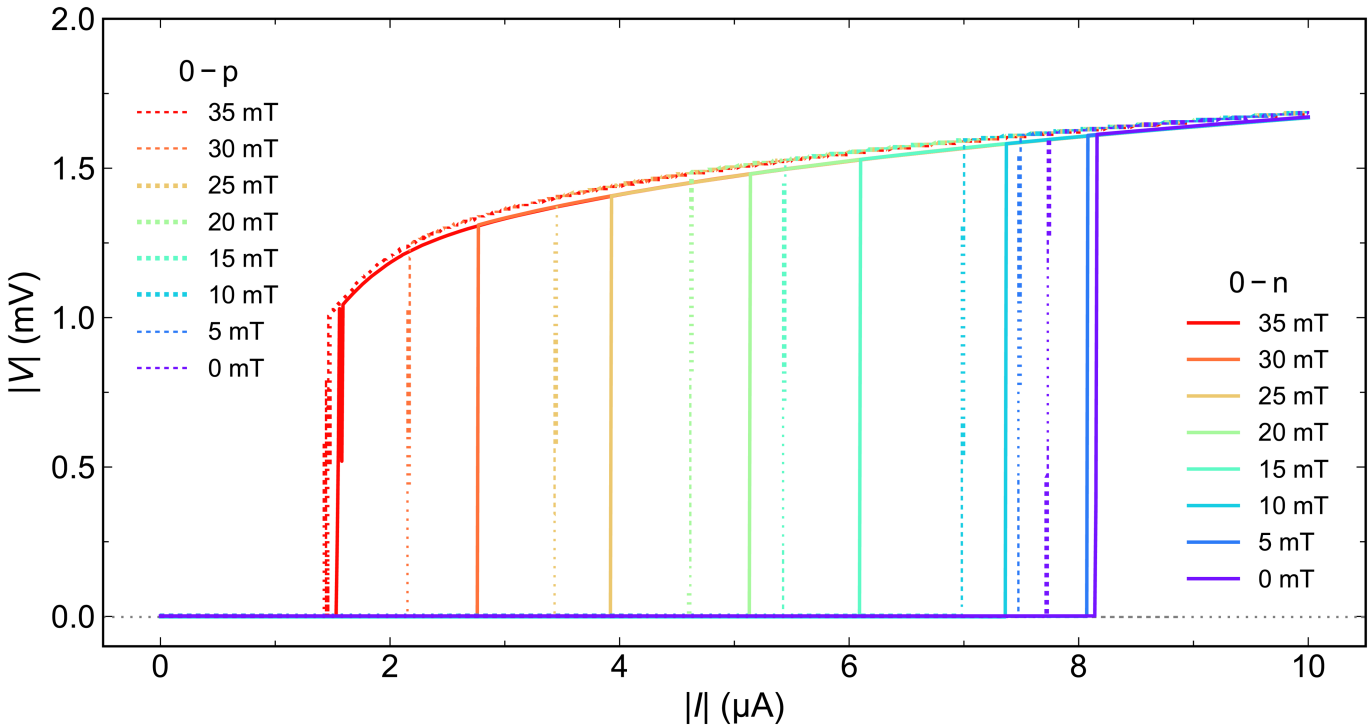

Extended Data Fig. 3 | *V-I* curves with 0-p and 0-n branches measured at different magnetic fields. Solid lines are 0-n branches (where I_{c-} was extracted) and dotted lines are 0-p branches (where I_{c+} was extracted) corresponding to Fig. 3. ΔI_c almost 'turns off' at 35 mT.

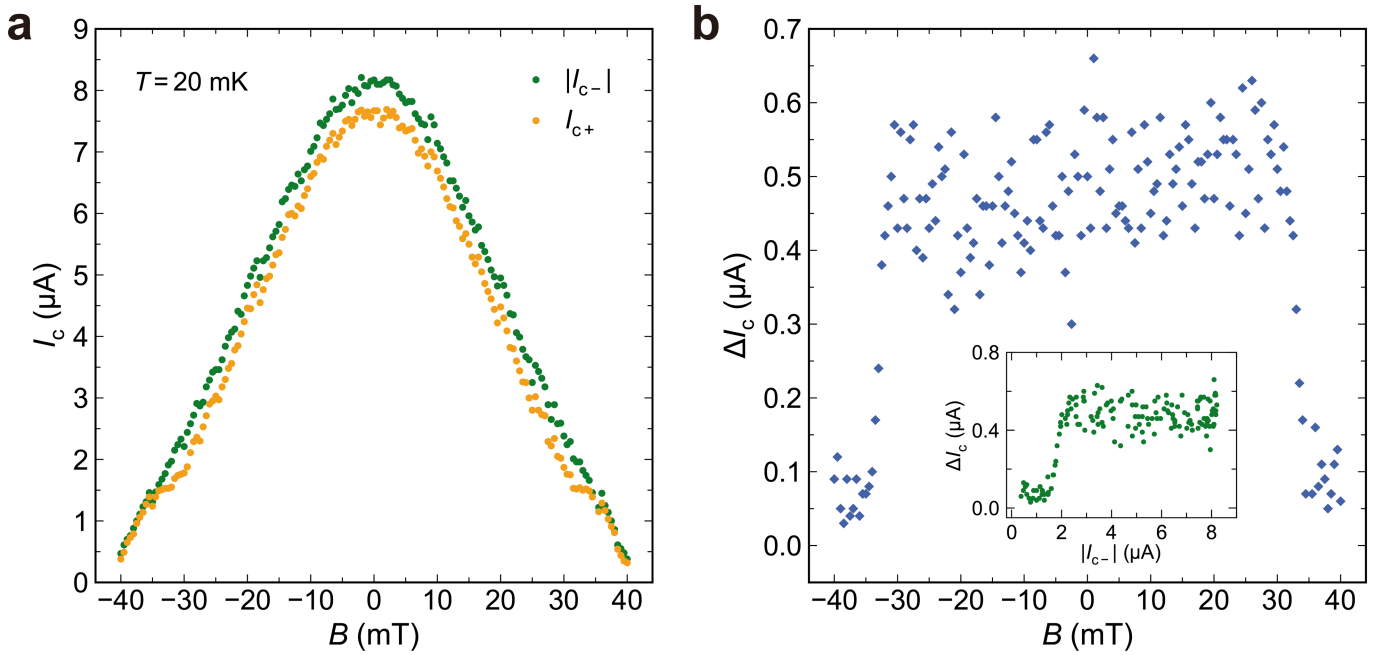

Extended Data Fig. 4 | Sweep-up magnetic field dependence of I_c and ΔI_c. **a**, I_{c+} (orange dots) and $|I_{c-}|$ (green dots) obtained from the 0-p and 0-n branches of the positive sweep as a function of applied magnetic field. The in-plane magnetic field was swept from negative to positive. **b**, ΔI_c as a function of magnetic field. Inset shows ΔI_c as a function of $|I_{c-}|$ from modulation of magnetic field with the diode effect 'turning off' below 2.1 μA. These sweep-up results are nearly identical with the sweep-down results shown in Fig. 3.

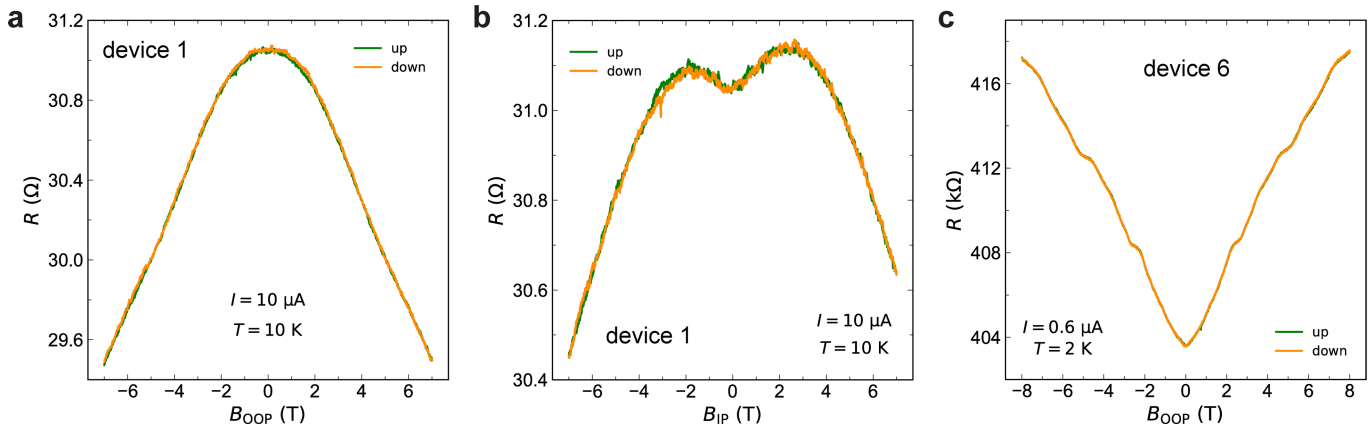

Extended Data Fig. 5 | Magnetoresistance of $NbSe_2/Nb_3Br_8/NbSe_2$ and FLG/Nb_3Br_8/FLG heterostructures. a, Sweep-up and sweep-down magnetoresistances of $NbSe_2/Nb_3Br_8/NbSe_2$ (device 1) with OOP magnetic field at 10 K (above T_c of $NbSe_2$). **b**, Sweep-up and sweep-down magnetoresistances of device 1 with in-plane magnetic field at 10 K. **c**, Sweep-up and sweep-down magnetoresistance of FLG/Nb_3Br_8/FLG (device 6) with OOP magnetic field at 2 K.

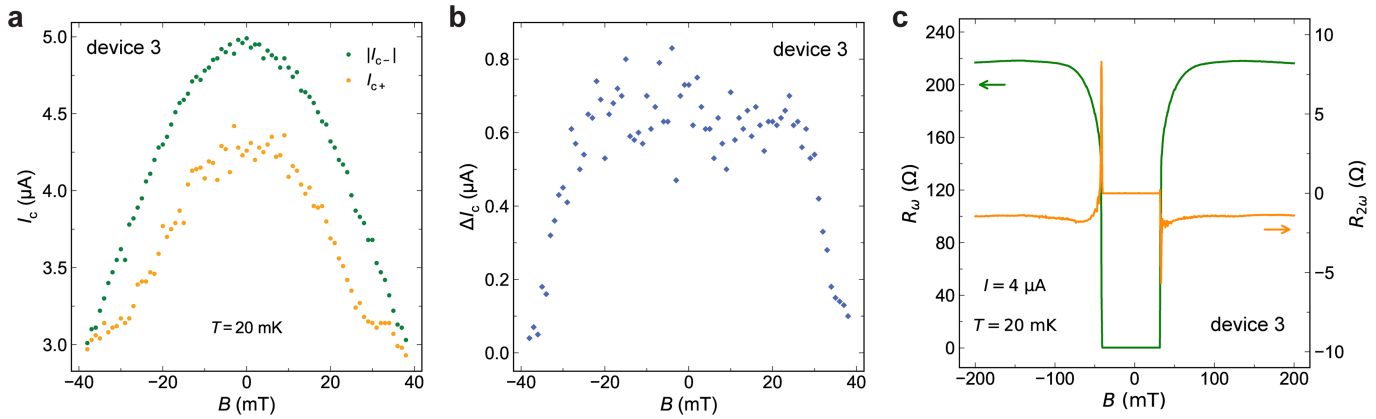

Extended Data Fig. 6 | Field-free Josephson diode effect of a $NbSe_2$/four-layer Nb_3Br_8/$NbSe_2$ device. a, I_{c+} and $|I_{c-}|$as a function of magnetic field at 20 mK in $NbSe_2$/four-layer Nb_3Br_8/$NbSe_2$ junction (device 3). **b**, ΔI_c as a function of magnetic field of device 3. **c**, First harmonic (R_ω) and second-harmonic resistances ($R_{2\omega}$) as a function of magnetic field measured at 20 mK with an applied current of 4 μA of device 3.

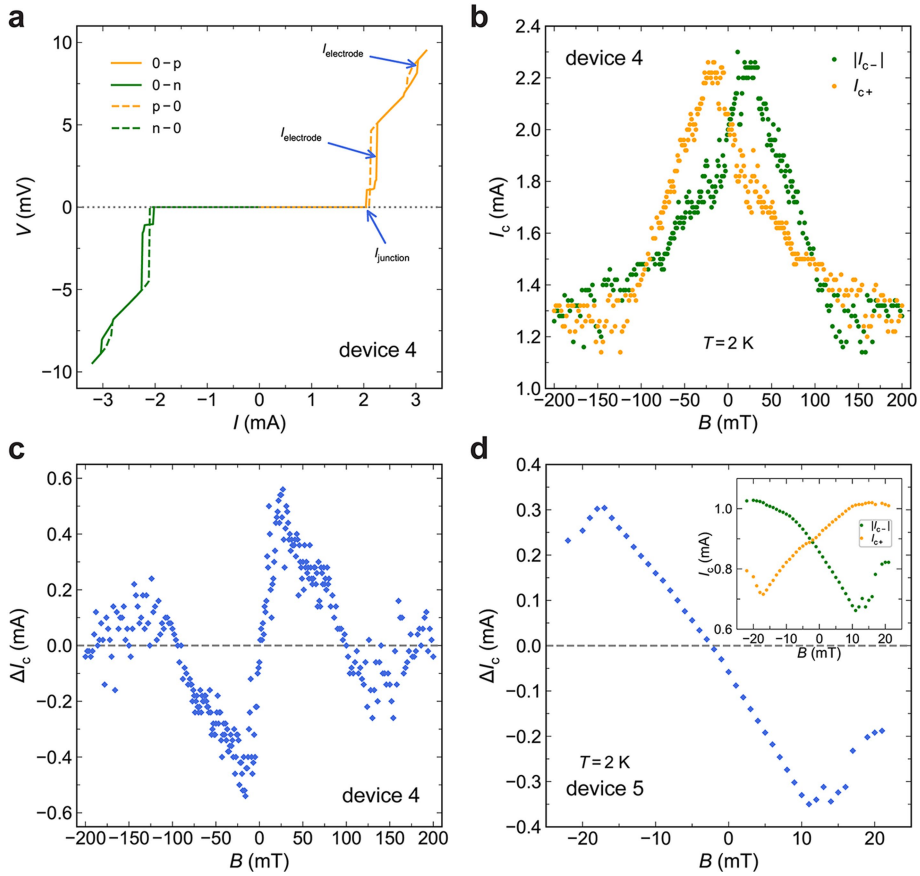

Extended Data Fig. 7 | Field-induced superconducting diode effect in $NbSe_2$/$NbSe_2$ and $NbSe_2$/FLG/$NbSe_2$ heterostructures. a, *V-I* curve of $NbSe_2$/$NbSe_2$ junction (device 4) measured at 2 K and 0 T. **b**, I_{c+} and $|I_{c-}|$ as a function of magnetic field of device 4 at 2 K. **c**, ΔI_c as a function of magnetic field of device 4. **d**, ΔI_c as a function of magnetic field of $NbSe_2$/FLG/$NbSe_2$ junction (device 5) measured at 2 K, inset shows the corresponding I_{c+} and $|I_{c-}|$.

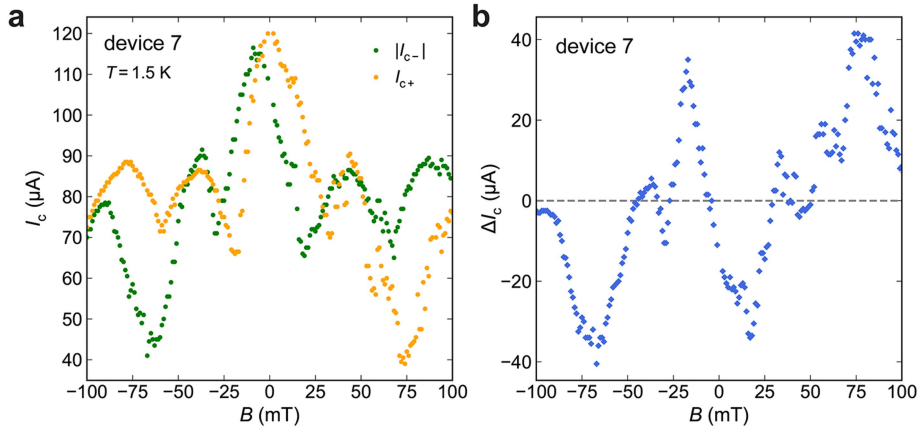

Extended Data Fig. 8 | Field-induced superconducting diode effect in $NbSe_2$/$NbSe_2$ heterostructures with a lower critical current. a, I_{c+} and $|I_{c-}|$ as a function of applied magnetic field of $NbSe_2$/$NbSe_2$ junction (device 7). **b**, ΔI_c as a function of magnetic field of device 7.

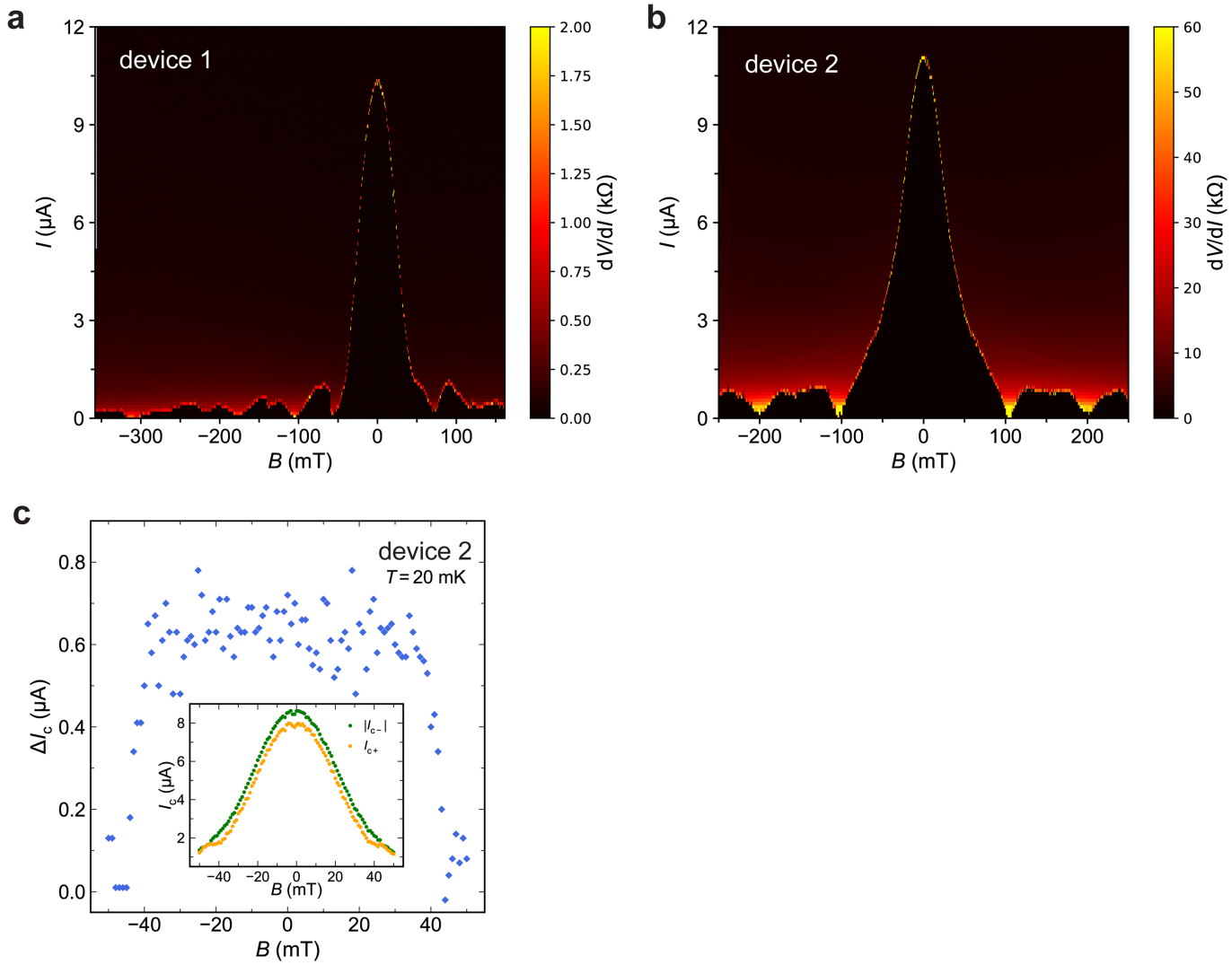

Extended Data Fig. 9 | Fraunhofer patterns of $NbSe_2/Nb_3Br_8/NbSe_2$ heterostructures. a, Fraunhofer pattern of device 1 with sweep-down magnetic field. **b**, Fraunhofer pattern of device 2. **c**, ΔI_c as a function of applied magnetic field of device 2 measured at 20 mK, inset shows the corresponding I_{c+} and $|I_{c-}|$.

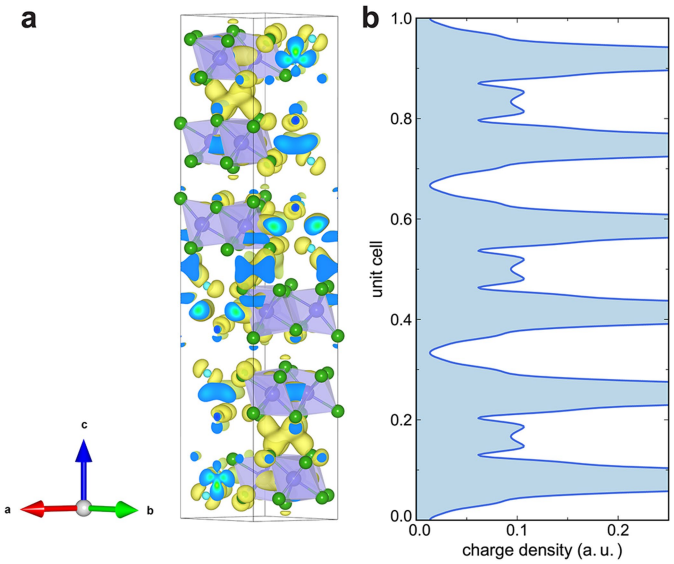

Extended Data Fig. 10 | Obstructed atomic insulator property of Nb_3Br_8. **a**, charge density distribution in a Nb_3Br_8 unit cell, the yellow/blue lobes indicate the charge density. **b**, charge density distribution as a function of unit cell location. Note the charge density does not drop to near zero in every other van der Waals gap.